High Frequency (4th order) Sequence Stratigraphy of Early Miocene Deltaic Shorelines, Offshore Texas and Louisiana

GCCC Publication Series #2019-10

M.I. Olariu
M. DeAngelo
D. Dunlap
R.H. Treviño

Keywords: stratigraphic, structural, capacity, wire-line log, seismic 3d, miocene, gulf wide, txla, amphistegina b, robulus l

Cited as:
M.I. Olariu, M. DeAngelo, D. Dunlap, R.H. Treviño, 2019, High frequency (4th order) sequence stratigraphy of Early Miocene deltaic shorelines, offshore Texas and Louisiana, Marine and Petroleum Geology, GCCC Publication Series #2019-10.

Bureau of Economic Geology
TEXAS Geosciences
Bureau of Economic Geology
Jackson School of Geosciences
The University of Texas at Austin

High frequency (4th order) sequence stratigraphy of Early Miocene deltaic shorelines, offshore Texas and Louisiana

Mariana I. Olariu*, Mike DeAngelo, Dallas Dunlap, and Ramon H. Treviño

Bureau of Economic Geology, the University of Texas at Austin, Austin, TX 78713, USA

*Corresponding author. Tel.: +1 512 475 7566; fax: +1 512 471 0140.

E-mail address: mariana.olariu@beg.utexas.edu

Keywords: Lower Miocene; growth fault; Gulf of Mexico; Lagarto; offshore

Abstract

Well logs and 3D seismic reflection data are integrated to image Lower Miocene depocenters of the upper Texas and westernmost Louisiana coastal and offshore areas. Although previously interpreted at a large scale (3rd order cycles), the detailed stratigraphy and depositional history of the early Miocene succession has not been fully developed. The upper lower Miocene interval from *Robulus L* (MFS10) to *Amphistegina B* (MFS9) has been further subdivided into five 4th order cycles (each 200 to 300 m thick) to provide finer scale stratigraphic detail and interpretation of depositional environments. Results of the finer scale correlations are presented in a series of sandstone percent maps. Overall, the maps display a strike-elongate (sub-parallel to the present day coastline) orientation for the sandstone bodies which thin to the southeast (basinward). Net sandstone thickness is relatively low in older cycles and increases in younger cycles suggesting an overall progradation of the deltaic system into the mapped area through time. Continued marine regression and southward movement of the shoreline are also confirmed by seismic amplitude

maps. After a major transgression associated with *Robulus L* deltaic progradation occurred under rising sea level conditions. Deltaic sediments prograded southward and sandstone brought to the upper Texas coast was distributed laterally by longshore currents to form strandplain coast lines. Maximum regression occurred during the interval MFS9_2 to MFS9_3 when a deltaic depocenter formed offshore Texas in east High Island area. However, sandstone thickness progressively decreased laterally to the east (offshore Louisiana) where more shale was present and marine processes reworked deltaic derived sandstones into shore parallel bars. There was a clear retreat of the shoreline during the youngest cycle marking the beginning of transgression associated with *Amphistegina B*. Detailed stratigraphic interpretation (at a 4th order scale) shows more variability in the dominant shoreline processes during early Miocene than previously thought. Recognition of sedimentary systems variability at a 4th order scale is critical for improved hydrocarbon exploration and in understanding potential future CO2 storage in the area.

Introduction

A thick wedge (about 3000 m) of siliciclastic Miocene age sediments underlies state and federal waters of offshore Texas and Louisiana (Morton et al., 1985; Galloway, 1989). Miocene sediments were deposited in an unstable basin along the northern margin of the Gulf of Mexico over a time interval of about 18 Ma (Galloway et al, 2000). The lower Miocene depositional episode lasted about 8 My from approximately 24 to 16 My (Fig. 1), encompassing the Aquitanian, Burdigalian, and early Langhian stages (Galloway et al., 1986; Galloway, 1989). Stratigraphically, the Lower Miocene is bounded at the base by the *Anahuac* shale and at the top by the *Amphistegina B* shale (Galloway et al., 2000) and consists of two major regressive cycles, known as the Oakville (LM1) and Lagarto (LM2) separated by an important, but less extensive transgressive episode associated

with *Marginulina A* (Fig. 1). Two widespread, transgressive deposits associated with *Amphistegina B* and *Textularia W* define the middle Miocene interval (Combellas-Bigott and Galloway, 2006). The upper Miocene depositional episode lasted for about 6.5 Ma (Galloway et al., 2000) and was terminated by a regional flooding event associated with the *Robulus E* biostratigraphic top (Fig. 1)

Many published studies provide analysis on the Miocene stratigraphy, structural style and depositional history at a regional scale (Rainwater, 1964; Kiatta, 1971; Galloway et al., 1986; Seni et al., 1994; Galloway et al., 2000), but high resolution stratigraphic interpretations have yet to be performed. Previous subsurface studies used seismic data and well log correlations to identify sediment dispersal patterns and main depocenters at a regional scale and over long time (million years) intervals (Rainwater, 1964; Kiatta, 1971; Galloway, 1989; Fillon and Lawless, 1999; Hentz and Zeng, 2003; Zeng and Hentz, 2003; Galloway et al., 2011). Due to the paucity of Miocene subsurface rock samples and the poorly consolidated nature of the sediment relatively few studies are based on core descriptions (Ambrose, 1990).

The Lower Miocene depositional sequence is the primary hydrocarbon producing zone in the Texas state offshore waters (Galloway et al., 1986; Seni et al., 1994). Early Miocene studies along the eastern Texas and western Louisiana coast have established the regional deltaic nature of the sediments (Rainwater, 1964; Kiatta, 1971; Galloway et al., 1986). Along the upper Texas coast and adjacent offshore region the lower Miocene comprises a thick (> 1000 m) wedge of terrigenous clastic sediments (Kiatta, 1971; Galloway, 1989). The Miocene along the southern Louisiana coast was deposited in a rapidly subsiding basin by the ancestral Mississippi river (Rainwater, 1964; Galloway et al., 2000). The upper Texas coast acted as an interdeltaic area with sediments delivered from Mississippi delta to the east via longshore currents (Galloway, 1990; Hunt and

Burgess, 1995; Galloway, 2000). Following the Anahuac transgression there was a southward movement of the shoreline (Kiatta, 1971) with minor shoreline fluctuations during Oakville (LM1) deposition. The lower Miocene maximum regressive shoreline position is reached during Lagarto (LM2) time (*Robulus L - Amphistegina B*) when sandstone was delivered to the shoreline from a deltaic depocenter in northeastern part of the High Island area (Kiatta, 1971).

The aim of the current research is to provide a detailed stratigraphic framework for the upper Lower Miocene from *Robulus L* to *Amphistegina B* along the upper Texas and westernmost Louisiana coast. Such a detail mapping is needed for (1) improved hydrocarbon exploration and (2) potential future storage of anthropogenic CO_2 because it occurs at optimal depths near areas with abundant anthropogenic sources of CO_2 (Treviño and Rhatigan, 2017). A broad understanding of the Miocene section of the northwest part of the Gulf of Mexico basin and the finer-scale sequence stratigraphic framework provide a high degree of precision often required in local areas for geologic characterization of future CO_2 sequestration prospects and should be considered for such detailed investigations (DeAngelo et al., 2019).

Geologic Setting

Early Miocene sediment influx exhibited an eastward shift of fluvial axes (Galloway et al., 2000; Galloway et al., 2011); the Houston sediment dispersal axis was abandoned in favor of the more easterly Red River axis which lies along the Texas-Louisiana border (Fig. 2). Principal depositional elements of the lower Miocene episode in the present-day Texas-Louisiana border area include the Calcasieu delta and Newton fluvial system (Galloway et al., 1986; Galloway, 1989). To the west, the Matagorda strandplain extended along the middle and much of the northeastern Texas coast (Fig. 2). To the east in Louisiana, deltaic progradation occurred along the Central Mississippi axis (Galloway et al., 2000). The Texas/Louisiana shore-zone system

developed between the Calcasieu Delta to the west and Central Mississippi delta to the east (Galloway et al., 2000). Well-developed shoreface sand bodies demonstrate large-scale strike transport of sediment from the adjacent Mississippi delta system (Galloway, 1989).

During the Early Miocene the Texas-Louisiana coastal region was structurally active (Ocamb, 1961; Doyle, 1979; Morton et al., 1985; Fillon and Lawless, 1999) with the development of coast-parallel growth faults and diapiric intrusions (Fig. 3). Offshore Texas major faults tend to strike northeast-southwest and are characterized by down-dip shortening into shale ridges that accommodate up-dip extension (Bradshaw and Watkins, 1994). The offshore of Louisiana is characterized by large-displacement listric growth faults that sole on a regional detachment zone above the Oligocene section (Edwards, 1994). Regional deformation is a product of salt mobilization from the level of the autochthonous Jurassic Louann Salt (Ocamb, 1961; Fillon and Lawless, 1999; Hentz and Zeng, 2003).

Amphistegina B shale marks the top of the lower Miocene and represents a major marine transgression throughout the region. A thick interval (over 600 m in the far down-dip areas) of sandstones interbedded with marine shales between *Robulus L* and *Amphistegina B* provides favorable conditions for multiple reservoirs to be stacked on the same structure (Kiatta, 1971; Galloway, 1989). The transgressive *Amphistegina* shale is thick enough (more than 900 m thick) in down-dip areas offshore to provide a seal for large fault traps (Kiatta, 1971; Galloway et al., 1986). The sequence from *Robulus L* to *Amphistegina B* consists of deltaic sediments which reflect continued marine regression and the progradation of a large early Miocene delta system (High Island Delta - Kiatta, 1971 or Calcasieu Delta - Galloway et al., 1986; Galloway, 1989) in the coastal and offshore area of the Texas-Louisiana border. The Calcasieu Delta, best developed in the Lagarto unit is interpreted as fluvial-dominated, wave influenced based on the sandstone body

geometry in the subsurface (Galloway, 1989). Narrow sandstone belts parallel to the present day coastline favored a wave-dominated interpretation for the High Island delta (Kiatta, 1971).

Data and Methodology

More than 1700 well logs with self-potential (SP) curves and a 3D seismic survey (Fig. 4) were used for detailed correlation and interpretation of the lower Miocene interval between *Robulus L* and *Amphistegina B*. Subsurface wire-line log correlations were performed using the genetic sequence approach of Galloway, 1989 because muddy intervals, such the regional *Amphistegina B* shale which are formed during marine transgressions, are easily identifiable (correlatable) on SP logs (Fig. 5). Self-potential values were normalized by rescaling all logs to correspond to a type of SP curve (-80 to +20 MV). Log normalization and cut-off values (-20 MV) helped to separate sandstone and shale in each log; sandstone lithologies have SP values between -80 to -20 MV in all wells. Mapping the sandstone body geometries in the subsurface enabled improved stratigraphic interpretation and recognition of depositional environments. In unstable settings, sandstone percentage maps rather than net sandstone thickness maps are used to locate depocenters and axes of sediment input as they are less affected by significant expansion of section across growth faults (Doyle, 1979; Galloway et al., 1982; Winker and Edwards, 1983). Log motif analysis was used for facies interpretation. Upward-coarsening log patterns interpreted as deltaic units and upward-fining motifs depicting shoreline transgressions were recognized in each log. The upper Lower Miocene interval was further subdivided into five 4^{th} order genetic stratigraphic cycles based on flooding surfaces MFS 9_1 to MFS 9_4 to provide finer scale stratigraphic detail. Due to the paucity of continuous Lower Miocene core, log patterns and sandstone percent maps together with

horizon slices through the seismic volume have been used as the most appropriate way to interpret depositional environments and to advance beyond previous studies.

The 3D seismic survey covers an area of about 3015 km^2 along the upper Texas and western Louisiana coast; bin spacing is 33 m and maximum vertical resolution is approximately 4 m. Seismic and well-log data were combined within Landmark's Decision Space Geosciences module to image stratigraphic surfaces. Four seismic horizons corresponding to the 4^{th} order maximum flooding surfaces were mapped (MFS 9_1 to MFS 9_4) between MFS 9 and MFS 10. The horizons were tracked manually in the seismic volume, gridded and contoured. Seismic attributes, such as minimum and root mean squares (RMS) amplitudes were extracted between the horizons of interest to provide information for interpreting depositional systems. Seismic amplitudes emphasize the variation in reflectivity and are sensitive to sandstone lithologies, which manifest as high values and therefore help image sandstone distribution and geological properties such as lateral discontinuities and changes in sediment thickness (Zeng and Hentz, 2003). Color-blended compositions of spectral attributes allow sub-seismic resolution observations of geological properties such as lateral discontinuities, and changes in sediment thickness. Seismic attributes (instantaneous amplitudes) can be used for detection of stratigraphic features, such as channels. Discontinuity attributes most often are applied to highlight structural features, such as faults and salt domes in a seismic volume, but are also useful in detecting subtle stratigraphic features in map view (Zeng and Hentz, 2003; Hart, 2008). Sweetness is derived by dividing reflection strength (instantaneous amplitude) by the square root of instantaneous frequency (Radovich and Oliveros, 1998; Hart, 2008) therefore highlighting areas containing higher amplitudes and lower frequencies (sandy intervals). Blending of different seismic attributes and applying transparency on seismic volumes makes it possible to identify hidden structural or depositional features (Hart, 2008).

Results

Structural deformation

Offshore Miocene strata are complexly faulted (Doyle, 1979; Galloway et al., 1982; Edwards, 1994), but good well control and seismic data helped with detailed structural mapping. Syn-sedimentary normal faults were recognized in the subsurface on seismic profiles (Fig. 7) or in well logs by missing or expansion of section (Fig. 5). About 300 faults have been mapped in the study area (Fig. 6). The faults strike generally northeast-southwest offshore Texas and west-east in Louisiana (Fig. 3). This results in arcuate fault trends concave toward the south approximately parallel to the present day coast line (Fig. 6). The density of faults is higher offshore Texas compared to Louisiana (Fig. 6). Normal faults have dips in excess of 60° in the upper part, but dips decrease to less than 30° or flatten with depth (Fig. 7). Seaward dipping normal faults offset stratigraphy and show thickened sedimentary units on their downthrown sides (Fig. 7B). Delta deposits are pierced by four salt diapirs in the study area (Fig. 6). Radial faulting forms around salt domes and appears to be post-depositional as there is little thickening across faults.

Sandstone maps

Self-Potential values between -90 and -20 MV were used to build both sandstone thickness and sandstone percent maps to illustrate sandstone body geometries and to interpret depositional environments. However, in growth-faulted settings, sandstone percentage maps are more useful to interpret depocenters and locate axes of sediment input as they remove the effect of differential subsidence and resulting thickness variations emphasize depositional control on lithofacies distribution (Galloway et al., 1982; Winker and Edwards, 1983). Therefore, sandstone percent maps are used in this study to show sandstone trends and outline the approximate positions of the

contemporaneous shoreline (Fig. 8). Five fourth-order sedimentary cycles (separated by 4 maximum flooding surfaces MFS 9_1 to MFS 9_4) with maximum thickness ranging from 235 m to 330 m have been identified within the Lagarto succession (about 1000 m thick) in High Island area (Fig. 5). The average sandstone thickness within each deltaic complex reaches about 40 to 70 m; the maximum thickness ranges from 140 to 210 m. Overall, the sandstone maps display a strike-elongate (sub-parallel to the present day coastline) geometry for the sandstone bodies (Fig. 8) which thin to the southeast (basinward). Net sandstone thickness is relatively low in the two older cycles above *Robulus L* (MFS 9_4 to MFS 10 and MFS 9_3 to MFS 9_4), increases throughout the middle cycles (MFS 9_2 to MFS9_3 and MFS 9_1 to MFS 9_2) and then decreases in the youngest cycle (MFS9 to MFS9_1) below the *Amphistegina B* shale.

Seismic geomorphology

3D seismic and well-log data were combined within Landmark's Decision Space Geosciences to map stratigraphic surfaces and investigate morphology of depositional systems. Seismic geomorphological analysis is based on amplitude maps generated from the horizons of interest (MFS 9_1 to MFS 9_4 between MFS 9 - *Amphistegina B* and MFS 10 - *Robulus L*). High seismic amplitudes represent sandstone lithologies (Fig. 9), whereas low to moderate amplitude values are indicative of finer-grained sediments. Color-blended compositions maps of spectral attributes allow sub-seismic resolution observations.

Seismic amplitude and color-blended composition maps demonstrate spatial variation and temporal evolution in sandstone trends and areal extent (Zeng and Hentz, 2003). Elongate sandstone bodies of the youngest interval (MFS9 to MFS9_1) are stretched in a WSW-ENE trend (Figs. 9A, 10A). Narrow (few km) strike-elongated sandstone belts are interpreted off southwest

Louisiana based on the presence of high seismic amplitudes; however, these are present only during the two youngest cycles (Figs. 9A, B and 10A, B). Two dip-elongated deltaic depocenters separated by mud are noticeable during the cycle from MFS9_1 to MFS9_2 (Figs. 9B, 10B). Seismic amplitude (Fig. 9C) and color blended composition maps (Fig. 10C) reveal sandstone accumulation in one strongly lobate and one strike-elongate depocenter during the cycle from MFS 9_2 to MFS 9_3. Discrete increases in amplitude are observed to form linear, shoreline-parallel ridges about 5 km wide and up to 60 km long (Figs. 9D, E and 10D, E) during the older intervals. The high-amplitude anomalies display a dominant NE–SW trend and are surrounded by lower seismic amplitudes interpreted as muddy sediments. Sandstone progressively decreases laterally to the east (offshore Louisiana) where more mud is present.

Discussion

Depositional systems variability

The stratigraphic interval from *Robulus L* to *Amphistegina B* (~2.5 Ma) in the study area has been previously interpreted either as a fluvial-dominated wave-influenced delta (Galloway, 1989) or as a wave-dominated delta (Kiatta, 1971); however, this paper shows that there is more variability in the dominant processes in time and space.

Mapping of log-interpreted (Fig. 8) and seismic (Figs. 9, 10) facies of the Miocene interval from *Robulus L* to *Amphistegina B* helped to outline the approximate positions of the contemporaneous shoreline. The increase in sandstone relative to shale upsection and a change from upward-coarsening successions to mostly blocky and upward-fining successions (Fig. 5) is interpreted to record deltaic progradation. Also the net sandstone thickness is relatively low in older cycles and increases in younger cycles (Fig. 8) suggesting an overall progradation of the deltaic system into the mapped area through time. Shore parallel elongation of the sandstone bodies in the subsurface

suggests an overall wave influence for the oldest and youngest cycles (Fig. 9). Wave and storm generated beaches lie on the flanks of the deltas away from the mouth of the distributary channels in the middle cycles which are more river-influenced (Figs. 9C, 10).

Normal faults and salt movement along the northern Gulf of Mexico margin have controlled the stratigraphy since the Cretaceous (Edwards, 1995), affecting deltaic processes as well. Numerous closely spaced growth faults (Figs. 6, 7) define the Miocene expansion zone offshore Texas (Winker 1982). Since buildup of sediments is associated with fault movements (Kiatta, 1971), a high density of faults offshore Texas (Fig. 6) indicates early Miocene deltaic depocenters in High Island which is also supported by sandstone trends obtained from amplitude and color-blended composition maps (Figs. 9, 10). A low fault density (Fig. 6) and a gradual decrease in sandstone thickness in southwest Louisiana (Fig. 9) suggest that the main Louisiana depocenters were further east and associated with the ancestral Mississippi delta (Morton et al., 1985; Galloway, 1989). To the west of and adjacent to the Mississippi delta system, abundant marine-reworked sediment fed strike-aligned barrier-strandplain systems (Morton et al., 1985; Galloway, 1989). The subsidence patterns of growth faults interfere with the relative sea level affecting shoreline processes (Winker and Edwards 1983; Ewing 1986; Olariu and Olariu, 2015). If the fault-induced subsidence is high, compared to relative eustatic and regional tectonic movements, local changes in deltaic processes occur (Olariu and Olariu, 2015). Such is the case of the sedimentary sequence of the Wilcox Group in Texas which shows a transition of depositional environments from tide-influenced and wave-modified to wave-dominated deltas as the shoreline approached the shelf edge during progradation (Olariu and Ambrose, 2016).

Five 4th order sequences (each about 300 m thick) were developed during early Miocene in the offshore area of Texas and Louisiana by the repeated regressive-transgressive transits of the

shoreline (Fig. 5). Sandstone morphologies show different architectures for successive deltaic complexes and an overall progradation to the southward followed by a shoreline retreat during the youngest cycle (Fig. 9). After a major transgression associated with *Robulus L*, deltaic progradation occurred under rising sea level conditions. Deltaic sediments brought to the upper Texas coast were distributed laterally by longshore currents to form strike-elongate bars (Fig. 9 D, E). Linear, parallel to the coast ridges with a dominant NE–SW trend developed above *Robulus L* during the two older cycles (MFS10 to MFS9_3). Sandstone gradually decreases laterally to the east (offshore Louisiana) where more mud is present. The shoreline remained roughly in the same position during the two older cycles (Fig. 9D, E).

Maximum regression occurred during the interval MFS9_2 to MFS9_3 when a deltaic depocenter formed in High Island area. There are clear dip-elongate geometries interpreted as fluvial distributaries (Figs. 9C, 10). Straight to slightly sinuous channels (NNW-SSE) fed river-dominated deltas (possibly with some tidal influence) downstream and favored southward progradation of strongly lobate shorelines (Fig. 10). Adjacent to the west, strike-elongate (NE-SW) features suggest increased wave reworking of the shoreline (Fig. 10B, D). Both the wave and fluvial-dominated deltaic successions are capped by the same flooding surface (Fig. 5) indicating autogenic changes in local depositional process regime. Many delta systems are a product of mixed-processes and tidal, fluvial or wave domination can vary even between individual lobes of the same delta (Olariu, 2014). Less fluvial discharge and presumably sediment flux favored more wave-reworking on the southern Danube lobe; the coeval northern lobe is fluvial-dominated with multiple distributary channels as is typical for fluvial-dominated deltaic morphology (Olariu, 2014).

Two sandy deltaic depocenters separated by a muddy interdeltaic area developed during the younger cycle from MFS9_1 to MFS9_2 (Fig. 9B). Straight to sinuous channels flowing NW-SE suggest a shifting in sediment delivery pathways and a tide or river-dominated morphology. There is a slight retreat of the shoreline during this cycle. Minor fault movement during transgression enhances the irregularity of the coast and favors tidal processes (Cumming and Arnot, 2005). The western depocenter has a more strike-oriented geometry suggesting wave-influence. Within a delta complex there may be several major distributaries that produce individual delta lobes (Kindiger, 1989). The presence of salt domes also affected deltaic progradation with sediments being diverted around the diapirs (Fig. 9B). The evolution of the growth faulted fluvial-dominated Lagniappe delta (Wisconsian of Gulf of Mexico) was controlled by salt diapirs uplifted along the shelf break (Kindiger, 1989; Roberts et al., 2004). The diapirs limited the basinward progradation of the delta and confined the sediments between the uplifts (Roberts et al., 2004) landward of the shelf edge, thereby reducing wave influence.

Narrow, elongate sandstone bodies of the youngest interval (MFS9 to MFS9_1) are stretched in a WSW-ENE trend (Fig. 9A). There is a clear retreat of the shoreline during the youngest cycle marking the beginning of transgression associated with *Amphistegina B.* Sandstone progressively decreases laterally to the east (offshore southernmost Louisiana) where more mud is present and marine processes rework deltaic derived sandstones into elongate bars parallel to the regional shoreline trend.

Fluctuations in sea level cause shifting in shoreline position and sedimentary axis (Galloway et al., 2000) accompanied by changes in the dominant processes (Vakarelov and Ainsworth, 2013). High variabilities of dominant processes in deltas during cross-shelf transits of the shoreline are well documented both for ancient (Bhattacharya and Walker, 1991; Galloway, 2001; Hampson et al.,

2011; Vakarelov and Ainsworth, 2013; Olariu and Ambrose, 2016; Ambrose et al., 2018) and modern systems (Morton, 1979; Kindiger 1989; Roberts et al., 2004; Ainsworth et al., 2011; Olariu, 2014). Wave processes are expected as deltas approach the shelf edge and also if accommodation is higher compared to river sediment supply unless waves are attenuated by shoreline morphology (Coleman and Wright, 1975; Porebski and Steel, 2006). The progradational to aggradational stacking pattern (Fig. 5) in the lower part of the succession above *Robulus L* indicates a significant relative sea level rise during accumulation (Porębski and Steel, 2006); retrogradational parasequences at the top of the succession below *Amphistegina B* suggest the onset of transgression and shoreline retreat. The presence of strongly lobate shorelines between MFS9_1 and MFS9_3 (Fig. 9) suggests a strong fluvial drive. The changes from wave domination to fluvial influence reflect significant variability of process regime during shoreline progradation (Fig. 9). The interplay between fluvial and wave-dominated shorelines (Fig. 9 B, C) is interpreted as autogenic response during the overall progradation of the deltaic complex.

Comparison with late Quaternary deltas

This study shows that Early Miocene 4th order deltaic depocenters have a spatial variability similar to late Quaternary depocenters along the northern part of the Gulf of Mexico (Fig. 11). The present day northern Gulf of Mexico margin receives sediments from more than 10 rivers (Fig. 11A) most of which form bay head deltas (Anderson et al.,2004); few of them (Mississippi, Rio Grande and Brazos) form large marine delta depocentres (Anderson et al., 2016). The distance between modern river valleys is less than 100 km (Fig. 11A). The summary of the last 120 ky of deposition along the Gulf margin shows a complex paleogeography with multiple deltaic depocenters at different locations on the shelf (Anderson et al., 2016). Multiple late Quaternary depocenters developed

during a single regressive-transgressive cycle (Anderson et al., 2004) resulting in a considerable variability of depositional environments along the margin (Fig. 11A) at a 4th order scale. The Lower Miocene paleogeographic reconstruction at a 3rd order scale (Galloway, 1989; Galloway et al., 2000) captures only the largest depocenters formed by stacking multiple 4th order sequences, but lacks the understanding of the depocenter dynamics at higher frequency cycles. Our detail mapping of multiple 4th order sequences identifies the individual depositional systems within the larger depocenters of Galloway and at a similar scale (dimensions, spacing, and thickness) with Late Quaternary depo-systems (Fig. 11). Although both fluvial-dominated the ancestral Colorado and Brazos deltas have distinct sizes and morphologies and occupy different positions on the shelf (Fig. 11A) during the same 4th order cycle due to differences in sediment supply (Anderson et al., 2016). The quaternary Rio Grande and Colorado deltas served as longshore sediment sources for the Central Texas shelf (Fig. 11A). In a similar way paleogeographic reconstructions of early Miocene deltas (Fig. 11B, C) display distinct delta lobes with different dominant regimes, either wave or fluvial-dominated indicating a high depositional process variability along strike. Based on our results (and despite the limited geographic coverage) we predict that early Miocene is similar to late Quaternary shoreline morphology in that multiple deltaic depocenters developed along the Gulf margin and produced distinct delta lobes with different dominant regimes. Therefore more detailed studies (4th order) are needed for a better depiction of depositional environments.

Conclusions

Well logs and 3D seismic reflection data were integrated to detail the stratigraphy and depositional history of the early Miocene succession of the upper Texas and westernmost Louisiana coastal and

offshore areas. Five 4th order sequences were formed by the repeated cross-shelf transits of the shoreline during the lower Miocene interval from *Robulus L* (MFS10) to *Amphistegina B* (MFS9). A series of percent sandstone maps display a strike-elongate (sub-parallel to the present day coastline) geometry for the sandstone bodies which thin basinward. Net sandstone thickness is relatively low in older cycles and increases in younger cycles suggesting an overall progradation of the deltaic system through time. Continued marine regression and southward movement of the shoreline are also reflected by seismic amplitude maps. Two main deltaic depocenters are centered in High Island area offshore Texas during the maximum regression. Sandstone progressively decreases laterally to the east in Louisiana where more shale is present and marine processes rework deltaic derived sandstones into shore parallel bars. The deltaic system moves landward during the youngest cycle marking the beginning of marine transgression associated with *Amphistegina B.*

Acknowledgements

This research was supported by the Department of Energy under DOE-NETL Award Numbers DE-FE0026083 and DEFE0029487. The authors are grateful to Seismic Exchange Inc. for providing 3D seismic data and to Landmark Graphics Corporation in the Landmark University Grant program. IHS Inc. provided access to its well and well- production database via Enerdeq® and to the Petra-integrated geoscience software application. The manuscript benefited from insightful comments from Robert Finley, associate editor Claudio Nicola Di Celma and reviewer Giacomo Dalla Valle. Publication authorized by the director of Bureau of Economic Geology, University of Texas at Austin.

Disclaimer: This report was prepared as an account of work sponsored by an agency of the United States Government. Neither the United States Government nor any agency thereof, nor any of their employees, makes any warranty, express or implied, or assumes any legal liability or responsibility for the accuracy, completeness, or usefulness of any information, apparatus, product, or process disclosed, or represents that its use would not infringe privately owned rights. Reference herein to any specific commercial product, process, or service by trade name, trademark, manufacturer, or otherwise does not necessarily constitute or imply its endorsement, recommendation, or favoring by the United States Government or any agency thereof. The views and opinions of authors expressed herein do not necessarily state or reflect those of the United States Government or any agency thereof.

References

Ainsworth, R. B., Vakarelov, B. K., and Nanson, R. A., 2011, Dynamic spatial and temporal prediction of changes in depositional processes on clastic shorelines: Toward improved subsurface uncertainty reduction and management: AAPG Bulletin, v. 95, p. 267-297.

Ambrose, W. A., Zeng, H., Zhang, J., Olariu M. I., Smith, D., and Clift, S., 2018, Depositional history and stratigraphic evolution of the Upper Wilcox Group and Reklaw Formation, northern Bee county, Texas, BEG RI 284, 87 p.

Ambrose, W. A., 1990, Facies heterogeneity and brine-disposal potential of Miocene barrier-island, fluvial and deltaic systems: Examples from Northeast Hitchcock and Alta Loma Fields, Galveston county, Texas, BEG Geological Circular 90, 35 p.

Anderson J. B., Wallace D.J., Simms A. R., Rodriguez A. B., Weight, R.W.R, and Taha, Z. P., 2016, Recycling sediments between source and sink during a eustatic cycle: Systems of late Quaternary northwestern Gulf of Mexico Basin, Earth-Science Reviews v. 153, p. 111–138.

Anderson, J.B., Rodriguez, A., Abdulah, K.C., Fillon, R.H., Banfield, L.A., McKeown, H.A., and Wellner, J.S., 2004, Late Quaternary stratigraphic evolution of the northern Gulf of Mexico: a synthesis. In: Anderson, J.B., Fillon, R.H. (Eds.), Late Quaternary Stratigraphic Evolution of the Northern Gulf of Mexico Margin. Society for Sedimentary Geology, Special Publication 79, pp. 1–23.

Bhattacharya, J. P., and Walker, R. G., 1991, River- and wave-dominated depositional systems of the Upper Cretaceous Dunvegan Formation, northwestern Alberta, Bulletin of Canadian Petroleum Geology, v. 39, p. 165–191.

Bradshaw, B. E. and Watkins, J. S., 1994, Growth Fault evolution in offshore Texas, Gulf Coast Association of Geological Societies Transactions 44, p. 103-110.

Coleman, J. M., and Wright, L. D., 1975, Modern River Deltas: Variability of Processes and Sand Bodies, in Broussard, M. L., ed., Deltas: Models for Exploration: Houston, Texas, Houston Geological Society, p. 99-149.

Combellas-Bigott, R. L. and Galloway, W. E, 2006, Depositional and structural evolution of the middle Miocene depositional episode, east-central Gulf of Mexico, AAPG Bulletin, v. 90, p. 335-362.

Cummings, D. I., and Arnott, R. W. C., 2005, Growth-faulted shelf-margin deltas: a new (but old) play type, offshore Nova Scotia: Bulletin of Canadian Petroleum Geology, v. 53, p. 211-236.

DeAngelo, M. V., Fifariz, R., Meckel,T. A., and R. H. Treviño, 2019, A seismic-based CO2-sequestration regional assessment of the Miocene section, northern Gulf of Mexico, Texas and Louisiana, International Journal of Greenhouse Gas Control, v. 81, p.29-37.

Diegel, F. A., J. F. Karlo, D. C. Schuster, R. C. Shoup, and P. R. Tauvers, 1995, Cenozoic structural evolution and tectono-stratigraphic framework of the northern Gulf coast continental margin, *in* M. P. A. Jackson, D. G. Roberts, and S. Snelson, eds., Salt tectonics: a global perspective: AAPG Memoir 65, p. 109–151.

Doyle, J. D., 1979, Depositional patterns of Miocene facies, middle Texas coastal plain, BEG RI 99, 28 p.

Edwards, M. B., 1994, Enhancing Sandstone Reservoir Prediction by Mapping Erosion Surfaces, Lower Miocene Deltas, Southwest Louisiana, Gulf Coast Basin, Gulf Coast Association of Geological Societies Transactions, v. 44, p. 205-215.

Edwards, M. B., 1995, Differential subsidence and preservation potential of shallow water Tertiary sequences, northern Gulf Coast Basin, USA, *in* Plint, G. A., ed., Special publications International Association of Sedimentology: *Wiley-Blackwell Publishing Ltd., Oxford, England,* v. 22, p. 265-281.

Ewing, T., 1986, Structural styles of the Wilcox and Frio growth fault trends in Texas: constraints on geopressured reservoirs: University of Texas at Austin, Bureau of Economic Geology Report of Investigation, v. 154, 86 p.

Fillon, R. H. and Lawless, P. N., 1999, Paleocene – Lower Miocene sequences in the Northern Gulf: Progradational slope salt-basin deposition and diminishing slope-bypass deposition in the deep basin, Gulf Coast Association of Geological Societies Transactions, v. 49, p. 224-241.

Galloway, W. E., Jirik, L. A., Morton, R.A., and DuBar, J. R., 1986, Lower Miocene (Fleming) Depositional Episode of the Texas Coastal Plain and Continental Shelf: Structural Framework, Facies, and Hydrocarbon Resources, BEG RI 150, 50 p.

Galloway, W. E., 1989 (a), Depositional framework and hydrocarbon resources of the early Miocene (Fleming) episode, northwest Gulf Coast Basin, Marine Geology, v. 90, p. 19-29.

Galloway, W. E., 1989 (b), Genetic Stratigraphic sequences in basin analysis II: Application to northwest Gulf of Mexico Cenozoic basin, AAPG Bulletin v. 73 (2), p. 143-154.

Galloway, W. E., Ganey-Curry, P. E., Li, X., and Buffler, R. T., 2000, Cenozoic depositional history of the Gulf of Mexico Basin, AAPG Bulletin 84 (11), p. 1743-1774.

Galloway, W.E., Whiteaker, T.L., Ganey-Curry, P., 2011. History of Cenozoic North American drainage basin evolution, sediment yield, and accumulation in the Gulf of Mexico basin. Geological Society of America Geosphere, 7 (2011), pp. 938-973.

Hart, B. S., 2008, Channel detection in 3-D seismic data using sweetness, AAPG Bulletin, v. 92 (6), p. 733-742.

Hentz, T. F. and Zeng, H., 2003, High-frequency Miocene sequence stratigraphy, offshore Louisiana: Cycle framework and influence on production distribution in a mature shelf province, AAPG Bulletin, v. 87, p. 197-230.

Hunt, J. L., and Burgess, G., 1995, Depositional styles from Miocene through Pleistocene in the north-central Gulf of Mexico: an historical reconstruction, Gulf Coast Association of Geological Societies Transactions, vol. 45, p. 275-284.

Kiatta, H. W., 1971, The stratigraphy and petroleum potential of the lower Miocene, offshore Galveston and Jefferson counties, Texas, Gulf Coast Association of Geological Societies Transactions, v. 21, p. 257-270.

Kindiger, J. L., 1989, Depositional history of the Lagniappe Delta, Northern Gulf of Mexico: Geo-Marine Letters, v. 9, p. 59-66.

Morton, R. A., 1979, Temporal and spatial variations in shoreline changes and their implications, examples from the Texas Gulf Coast, Journal of Sedimentary Petrology, vol. 49, p. 1101-1112.

Morton, R. A., Jirik, L.A., and Foote, R. Q., 1985, Depositional history, facies analysis, and production characteristics of hydrocarbon-bearing sediments, offshore Texas, Geological Circular 85-2, 31 p.

Ocamb, R. D., 1961, Growth faults of South Louisiana, Gulf Coast Association of Geological Societies Transactions, vol. 11, p. 139-175.

Olariu, M. I., and Ambrose, W. A., 2016, Process regime variability across growth faults in the Paleogene Lower Wilcox Guadalupe delta, South Texas Gulf Coast, Sedimentary Geology, v. 341, p. 27-49.

Olariu, M. I., and Olariu C., 2015, Ubiquity of wave-dominated deltas in outer shelf growth faulted compartments, JSR, v. 85, p.768-779.

Olariu, C., 2014, Autogenic process change in modern deltas: lessons for the ancient: International Association of Sedimentologists, Special Publication, v. 46, p. 149-166.

Porębski, S. J., and Steel, R. J., 2006, Deltas and sea-level change: Journal of Sedimentary Research, v. 76, p. 1-14.

Radovich, B. J., and R. B. Oliveros, 1998, 3-D sequence interpretation of seismic instantaneous attributes from the Gorgon field: The Leading Edge, v. 17, p. 1286–1293.

Rainwater, E. H., 1964, Regional stratigraphy of the Gulf Coast Miocene, Gulf Coast Association of Geological Societies Transactions., v. 14, p. 81-124.

Roberts, H. H., Fillon, R. H., Kohl, B., Robalin, J., and Sydow J., 2004, Depositional architecture of the Lagniappe Delta: Sediment characteristics, timing of depositional events, and temporal relationship with adjacent shelf-edge deltas, in Anderson J. B. and Fillon R. H., eds., Late Quaternary Stratigraphic Evolution of the Northern Gulf of Mexico Basin: SEPM Special Publication, v. 79, p. 143-188.

Seni, S. J., Desselle, B. A., and Standen, A., 1994, Scope and Construction of a Gas and Oil Atlas Series of the Gulf of Mexico: Examples from Texas Offshore Lower Miocene Plays, Gulf Coast Association of Geological Societies Transactions 44, p. 681-690.

Treviño, R. H., and J. L. Rhatigan, 2017, Chapter 1: Regional Geology of the Gulf of Mexico and the Miocene Section of the Texas Near-Offshore Waters, in R. H. Trevino, and T. A. Meckel, eds., Geological CO2 Sequestration Atlas for Miocene Strata Offshore Texas State Waters: Report of Investigations, The University of Texas at Austin, Bureau of Economic Geology, p. 3-6.

Vakarelov, B. K., and Ainsworth, R. B., 2013, A hierarchical approach to architectural classification in marginal-marine systems: Bridging the gap between sedimentology and sequence stratigraphy, AAPG Bulletin, v. 97, p. 1121-1161.

Winker, C. D., and Edwards, M. B., 1983, Unstable progradational clastic shelf margins, in Stanley, D. J., and Moore, G. T. (eds.), The shelfbreak— Critical interface on continental margins, SEPM Special Publication 33, p. 139–157.

Winker, C. D., 1982, Cenozoic shelf margins, northwestern Gulf of Mexico basin: Gulf Coast Association of Geological Societies Transactions 32, p. 427-448.

Zeng, H., and Hentz, T. F., 2003, High-frequency sequence stratigraphy from seismic sedimentology: Applied to Miocene, Vermilion block 50, Tiger Shoal area, offshore Louisiana, AAPG Bulletin, v. 88, p. 153-174.

Figure Caption

Figure 1. Correlation chart showing lithostratigraphic and biostratigraphic subdivisions of the Miocene section of the northwest shelf of the Gulf of Mexico (modified from Galloway et al., 1986) The early Miocene depositional episode lasted for about 8 Ma (from 16 to 24 Ma) and is bounded by the *Anahuac* and *Amphistegina B* shale. Two major regressive cycles, Oakville (LM1) and Lagarto (LM2) are separated by an important, but less extensive transgressive episode associated with *Marginulina A.*

Figure 2. Paleogeographic map depicting distribution of principal early Miocene depositional environments (modified from Galloway, 1989). In south Texas the lower Miocene depositional framework includes the Santa Cruz fluvial system and the wave-dominated North Padre delta. Extensive wave-reworking nourished Matagorda strandplain. The Texas/Louisiana shore-zone system connects the Calcasieu Delta to the west and Central Mississippi delta to the east.

Figure 3. Regional structural framework (modified from Diegel et al., 1995) showing the Miocene expansion zone in the offshore area of Texas and Louisiana (study area highlighted in red, present day coast line shown in cyan) Early Miocene structural elements consist of numerous closely spaced coast-parallel growth faults (purple lines) and diapiric intrusions such as salt domes (shown in pink).

Figure 4. Map of the study area showing wells and primary 3D seismic dataset (highlighted in orange) The state - federal waters boundary is demarcated by the blue line subparallel to the coast (note that Texas state waters are wider than those of Louisiana) Subsurface control consisted of about 1000 wells; dip and strike cross-sections (AA', BB') and seismic reflection profiles (CC', DD') shown in red.

Figure 5. Regional well log cross-sections showing the Miocene succession of the upper Texas and westernmost Louisiana coastal and offshore areas (for location see Fig. 4). The interval between MFS 10 (*Robulus L)* and MFS 9 *(Amphistegina B)* has been subdividided into five 4th order genetic stratigraphic cycles based on flooding surfaces MFS 9_1 to MFS9_4 to provide finer scale stratigraphic detail. A cutoff value of -20 Mv was used to separate sand from shale in each well. A**.** Dip-oriented structural cross-section. Multiple normal faults offset the stratigraphy. B. Strike-oriented stratigraphic (flattened at MFS 9) cross-section.

Figure 6. Regional structural setting - depth structure maps A. MFS 9 B. MFS 10 (warm colors - shallow; cool colors – deep) showing about 300 faults and 4 salt domes in the study area The faults

strike northeast-southwest and have arcuate trends concave toward the south approximately parallel to the present day coast line (note that the area offshore Louisiana is less faulted). Radial faulting forms around salt diapirs.

Figure 7. Seismic reflection profiles A. strike-oriented (VE = 3) B. dip-oriented (no vertical exaggeration) showing how growth faults and salt diapirs affect Miocene stratigraphy in the study area (for location see Fig. 4). Faults have dips in excess of 60° in the upper part, which decrease to less than 30° or flatten with depth. Seaward dipping normal faults offset stratigraphy and show thickened sedimentary units on their downthrown sides. C. Close-up of strike-oriented profile and D. Close-up dip-oriented profile showing maximum flooding surfaces separating 4th order cycles between MFS 9 and MFS 10. Seismic data owned (controlled) by Seismic Exchange, Inc.; interpretation is that of the Bureau of Economic Geology.

Figure 8. Sandstone percent maps of the Lower Miocene interval from MFS 9 to MFS 10 Overall, the maps display a strike-elongate (sub-parallel to the present day coastline) geometry for the sandstone bodies which thin to the southeast (basinward). The average sandstone thickness within each deltaic complex ranges from about 40 to 70 m. Net sandstone thickness is relatively low in older cycles and increases in younger cycles suggesting an overall progradation of the deltaic system into the mapped area through time.

Figure 9. Seismic amplitude maps showing the spatial variation and temporal evolution in sandstone trends and areal extent of depocenters during late Lower Miocene A. MFS 9 to MFS 9_1 (youngest cycle) B. MFS 9_1 to MFS 9_2 C. MFS 9_2 to MFS 9_3 D. MFS 9_3 to MFS 9_4 E. MFS 9_4 to MFS 10 (oldest cycle). High reflectivity values (warm colors) represent sandstone, whereas low to moderate amplitudes are indicative of finer-grained sediments. Seismic data owned (controlled) by Seismic Exchange, Inc.; interpretation is that of the Bureau of Economic Geology.

Figure 10. Paleoshoreline positions and distribution of depocenters during the maximum regression interval from MFS 9_2 to MFS 9_3 A. Uninterpreted (faults highlighted in black) B. Interpreted sweetness attribute maps. C. Uninterpreted (faults highlighted in black) D. Interpreted color-blended composition of spectral attributes (instantaneous amplitude, discontinuity, sweetness) allows sub-seismic resolution observations of geological properties such as lateral discontinuities in sandstone trends (depocenters). Straight to slightly sinuous channels (NNW-SSE) fed river-dominated deltas and favored southward progradation of strongly lobate shorelines. Adjacent to the west, strike-elongate (NE-SW) features (dashed line) suggest increased wave reworking of the shoreline. High reflectivity values (warm colors) represent sandstone, whereas low to moderate amplitudes are indicative of finer-grained sediments. E. F. Strike-oriented seismic reflection profiles passing through the two interpreted fluvial channels (highlighted in red; position of cross-sections indicated in B). Seismic data owned (controlled) by Seismic Exchange, Inc.; interpretation is that of the Bureau of Economic Geology.

Figure 11. Comparison of Early Miocene with Late Quaternary depositional systems A. Paleogeographic reconstruction of quaternary deltaic depocenters (Rio Grande, Colorado, Brazos and ancestral Mississippi) along the northern margin of the Gulf of Mexico (modified from Anderson et al., 2016) Paleogeographic maps of Early Miocene showing depositional

environments during B. MFS9_1 - MFS9_2 and C. MFS9_2 - MFS9_3 cycles. Wave reworking of the shoreline is interpreted from seismic data on the western flank of the fluvial delta in B. and inferred for the eastern flanks in B. and C.

Figure 1

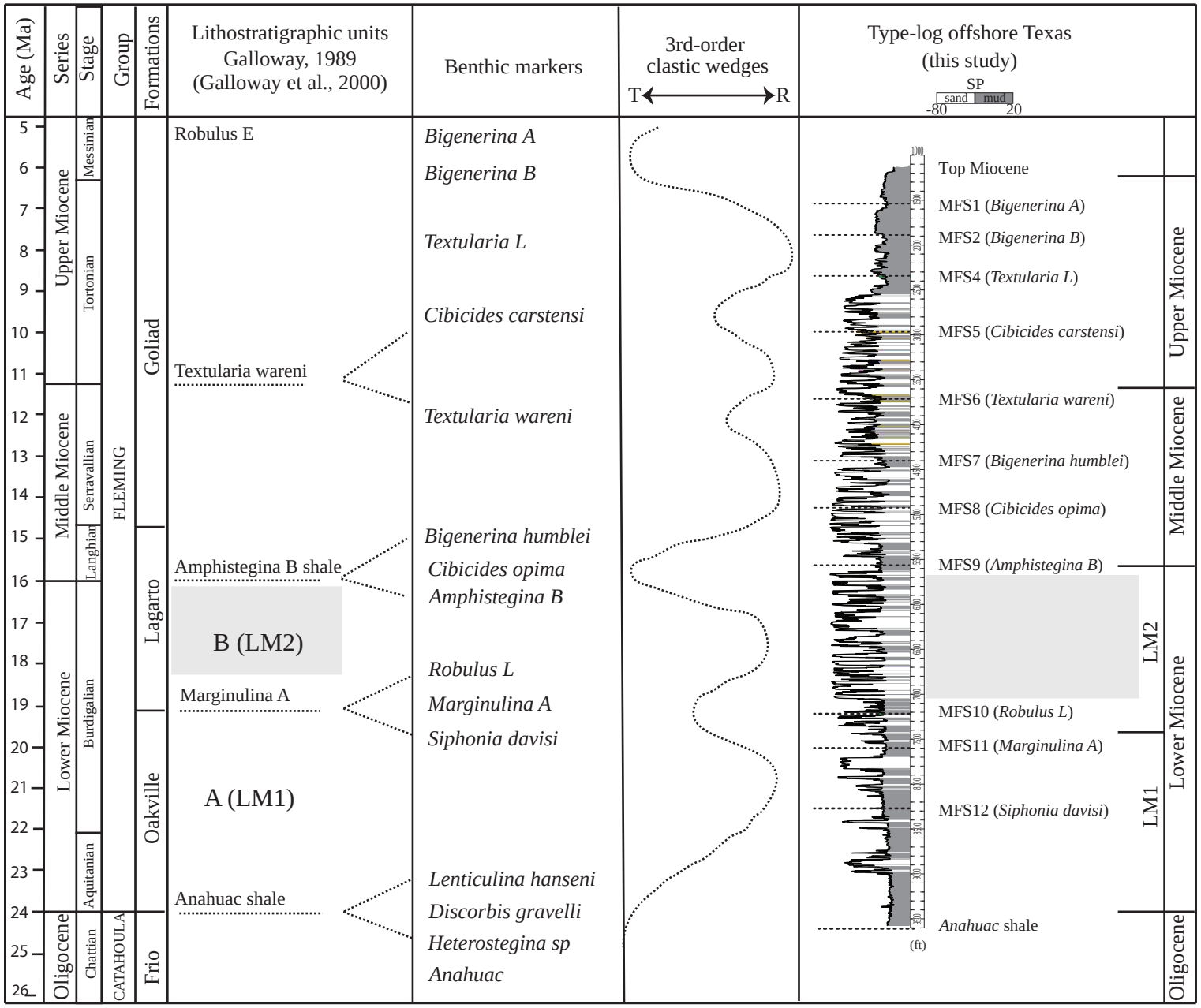

Figure 1. Olariu_et _al.2019

Figure 2

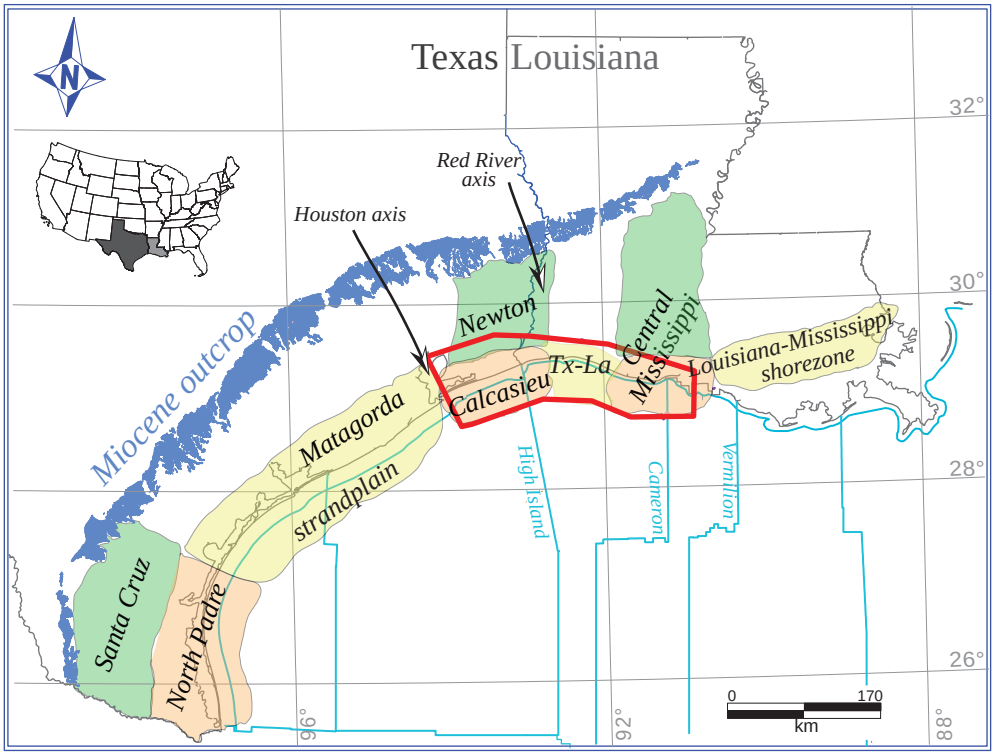

Figure 2. Olariu_et_al.2019

Figure 3

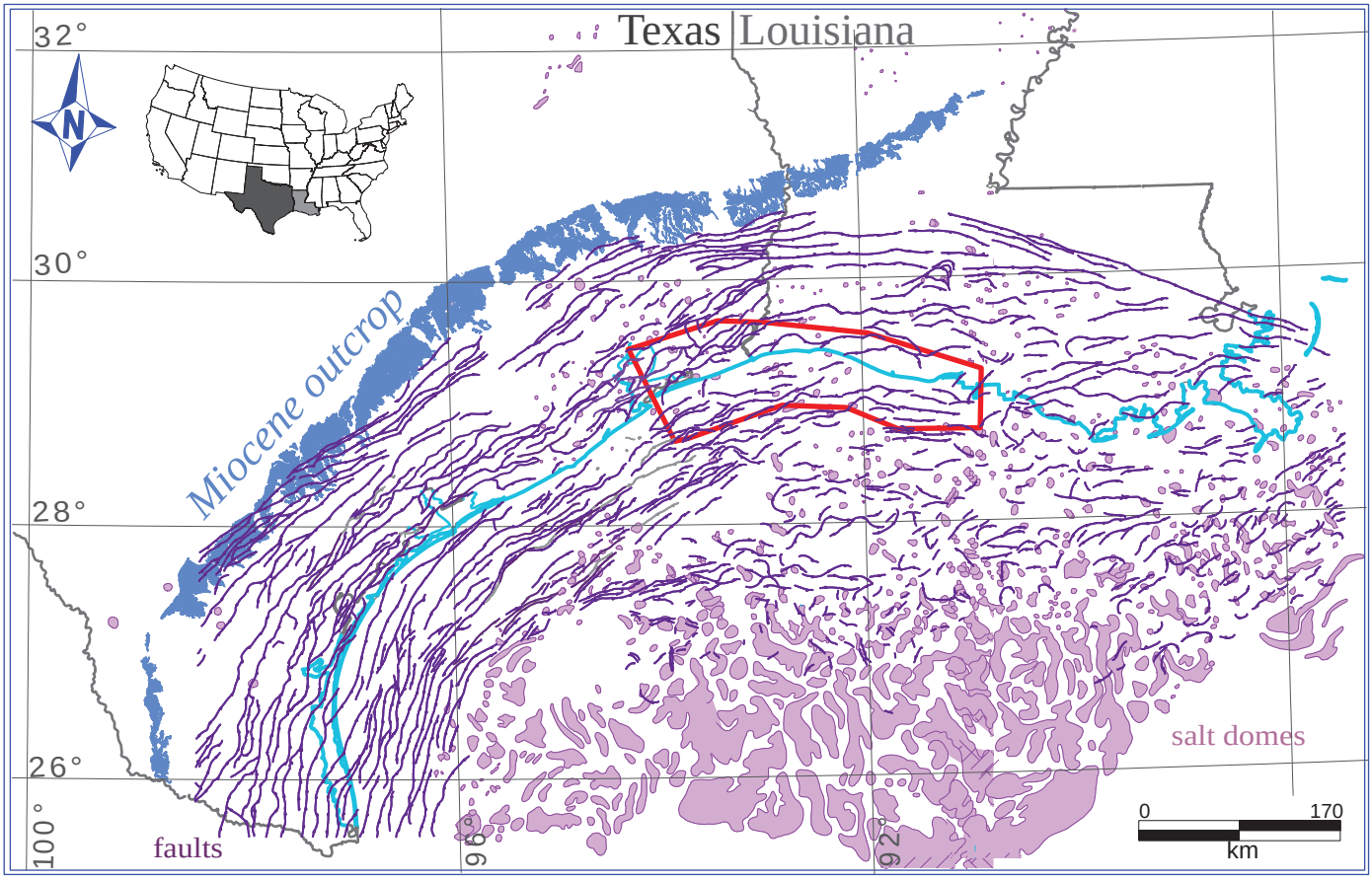

Figure 3. Olariu_et_al.2019

Figure 4

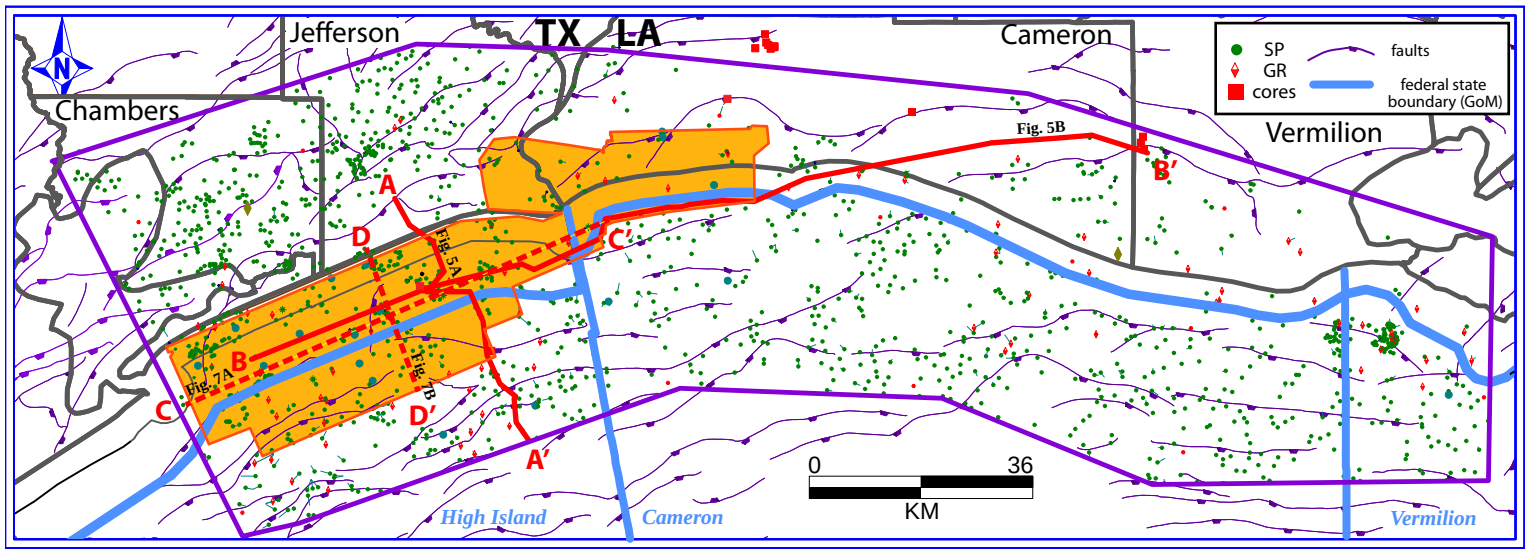

Figure 4. Olariu_et_al.2019

Figure 5

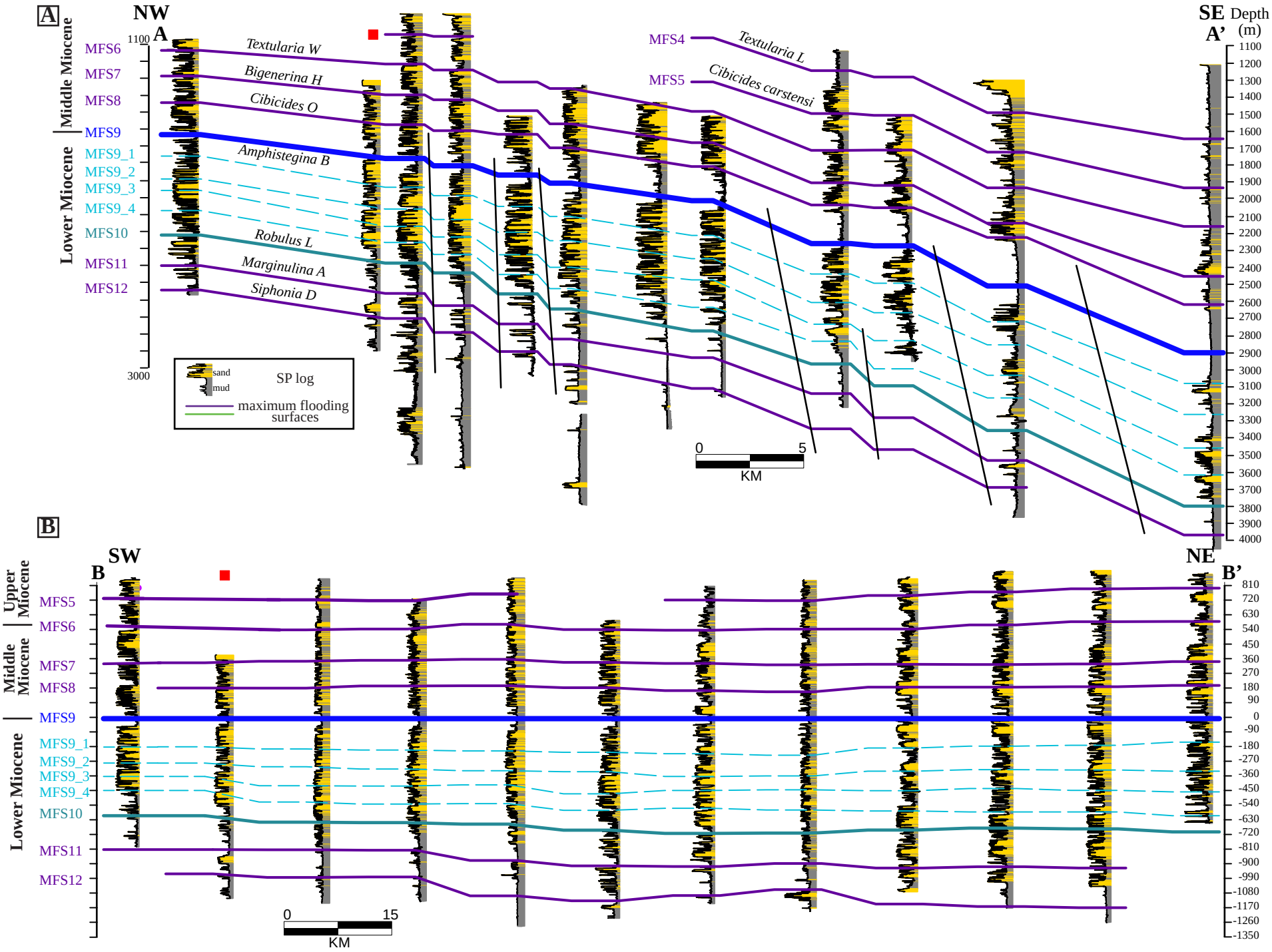

Figure 5. Olariu_et_al.2019

Figure 6

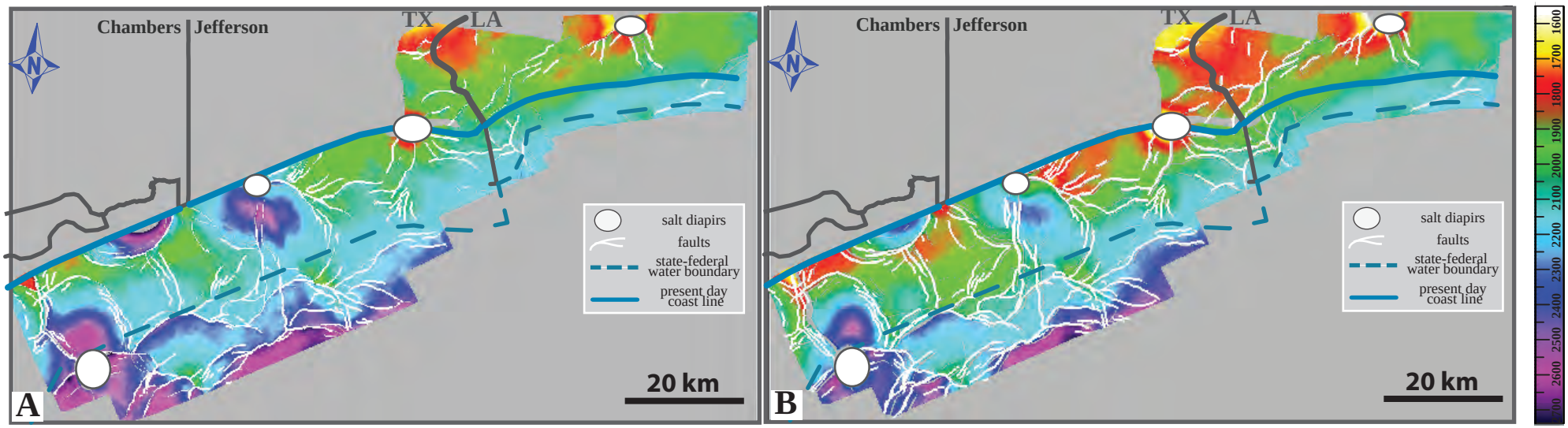

Figure 6. Olariu_et_al.2019

Figure 7

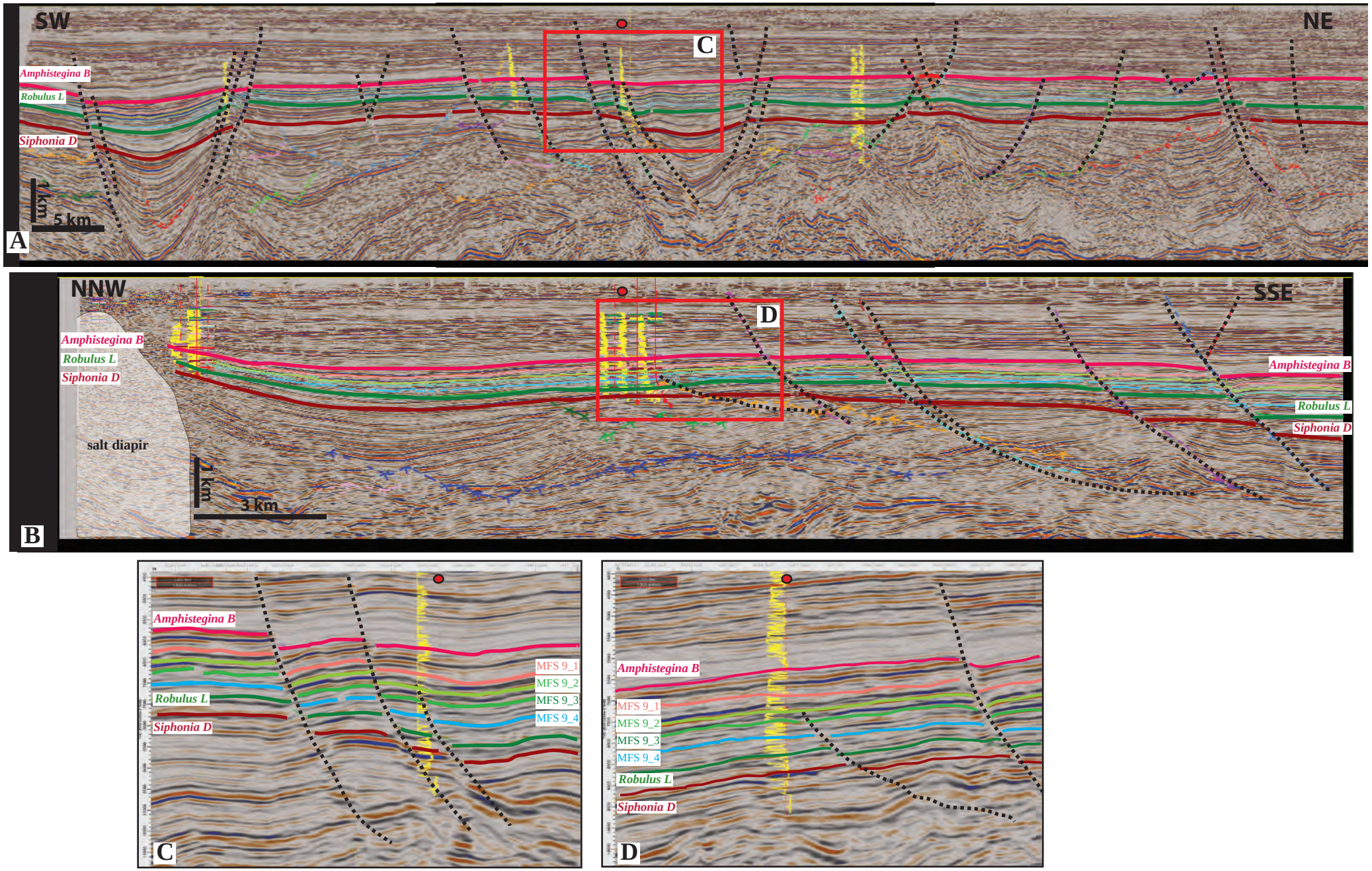

Figure 7. Olariu_et_al.2019

Figure 8

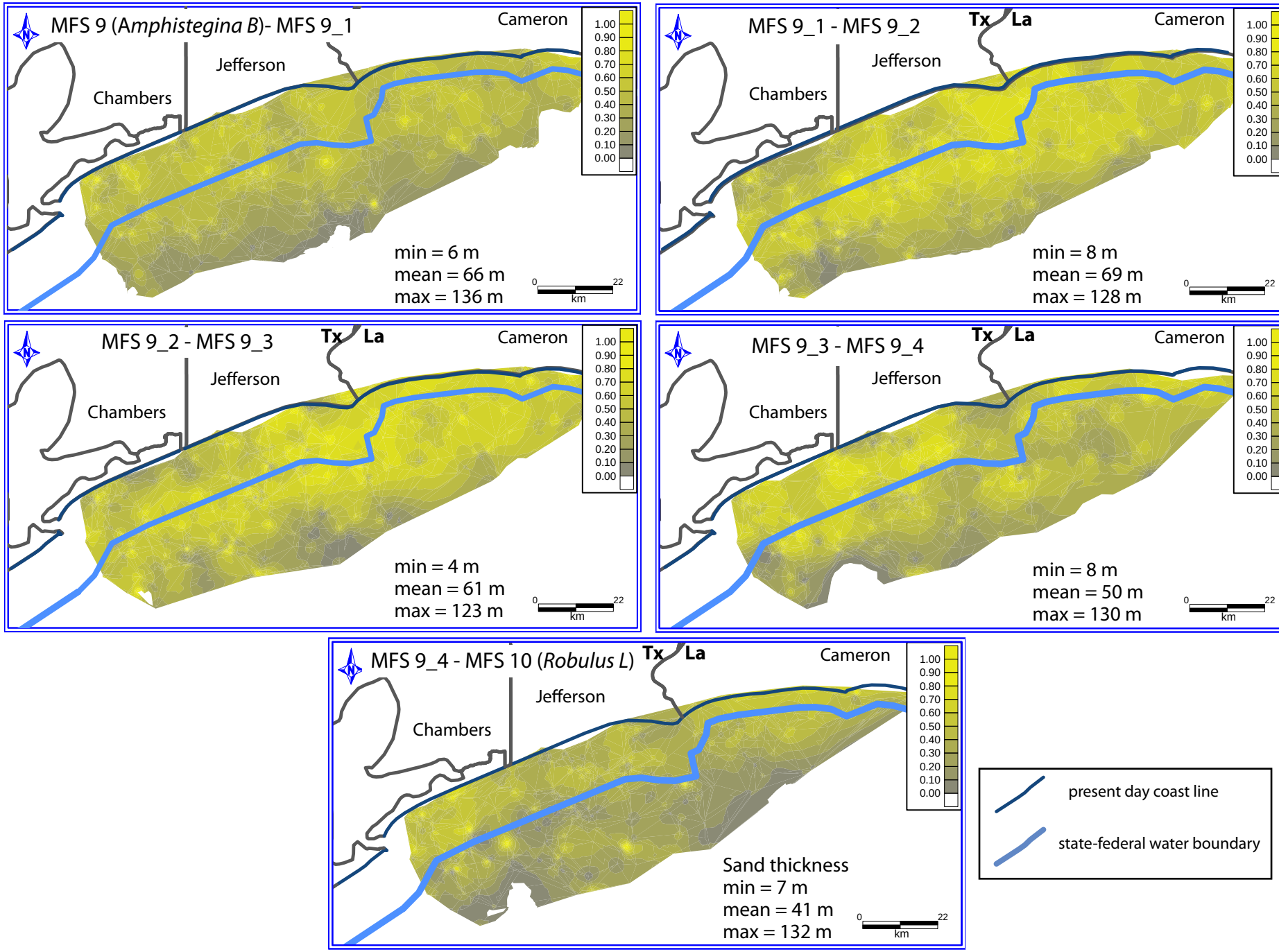

Figure 8. Olariu_et_al.2019

Figure 9

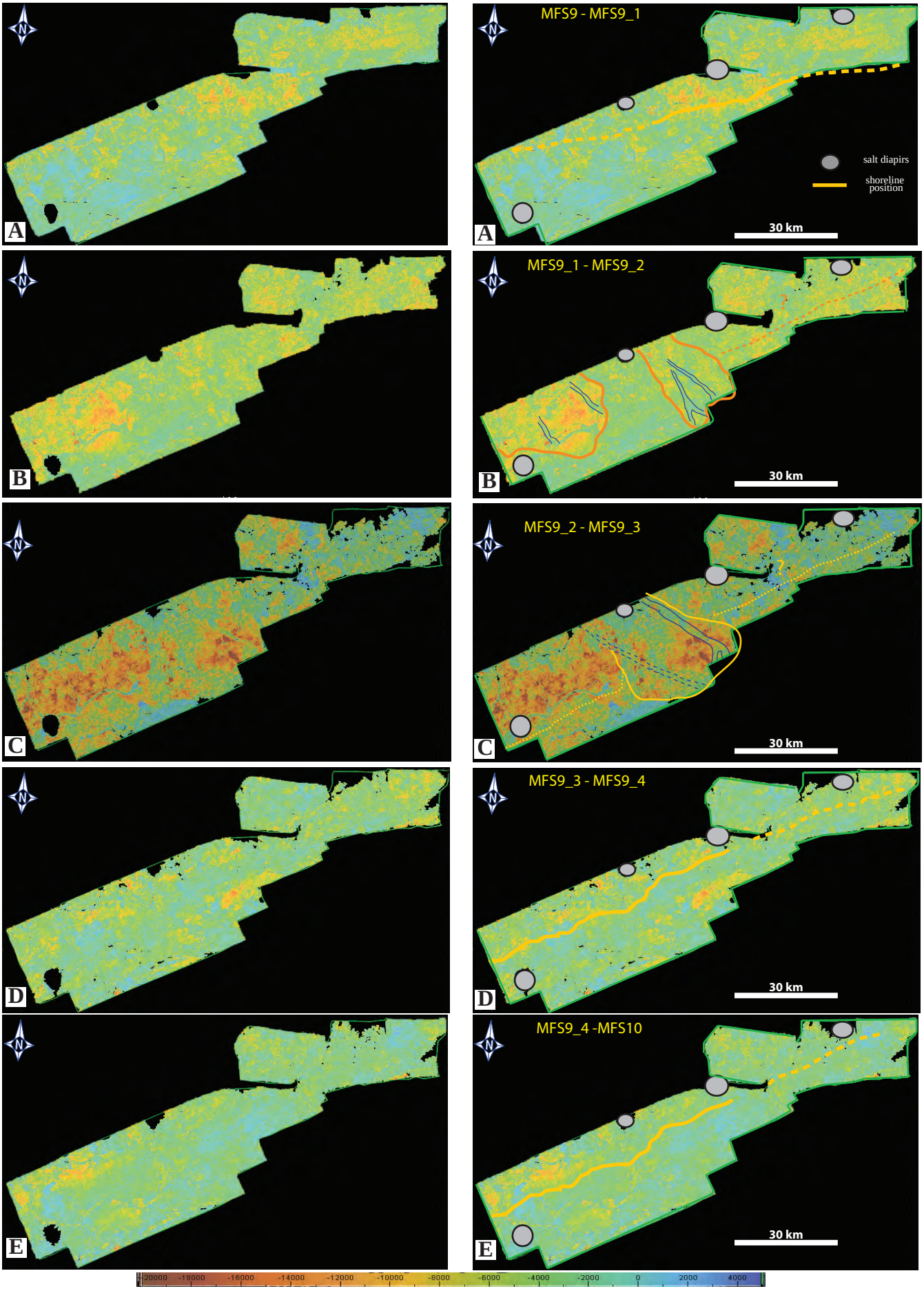

Figure 9. Olariu_et_al.2019

Figure 10

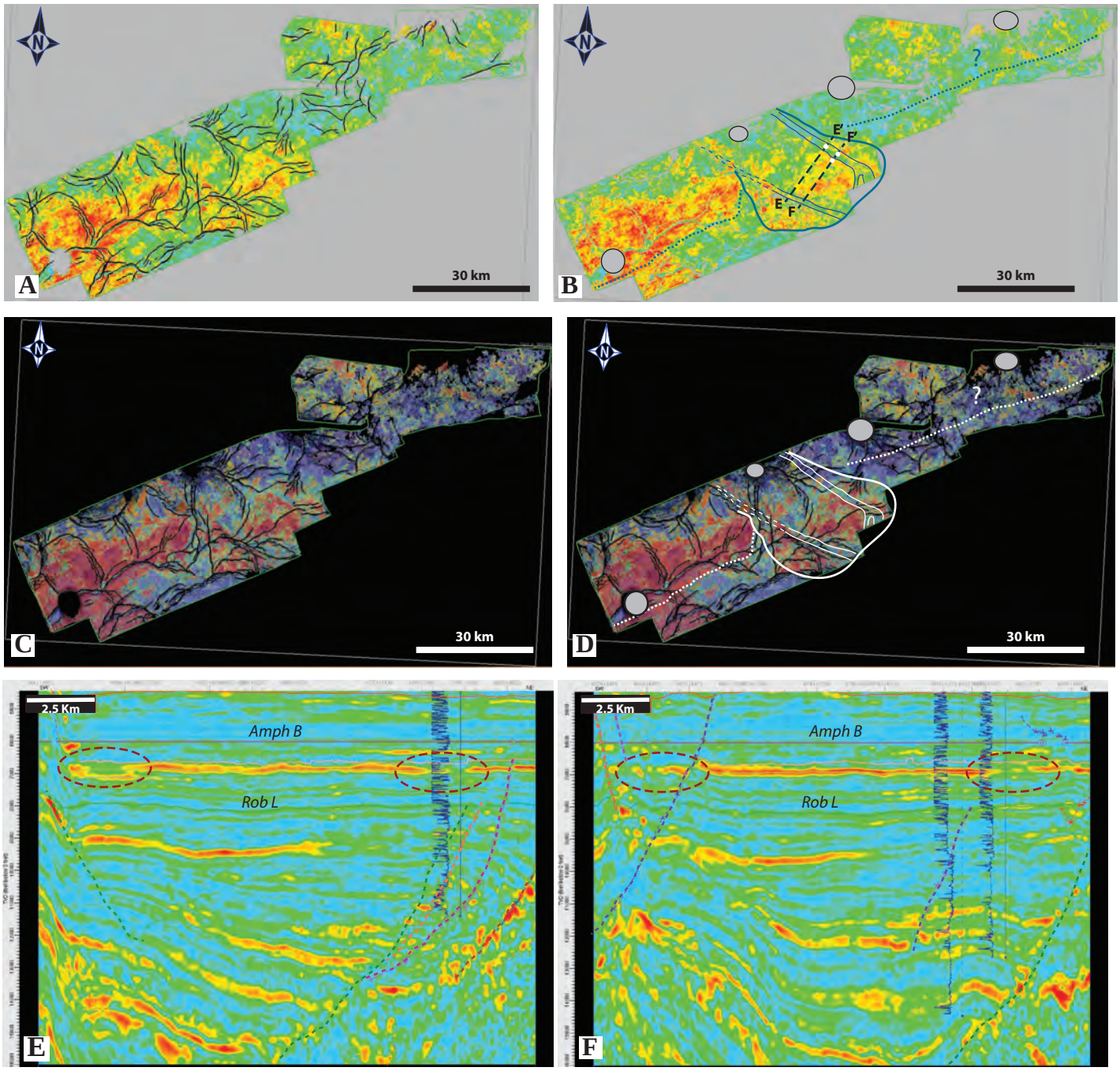

Figure10. Olariu_et_al.2019

Figure 11

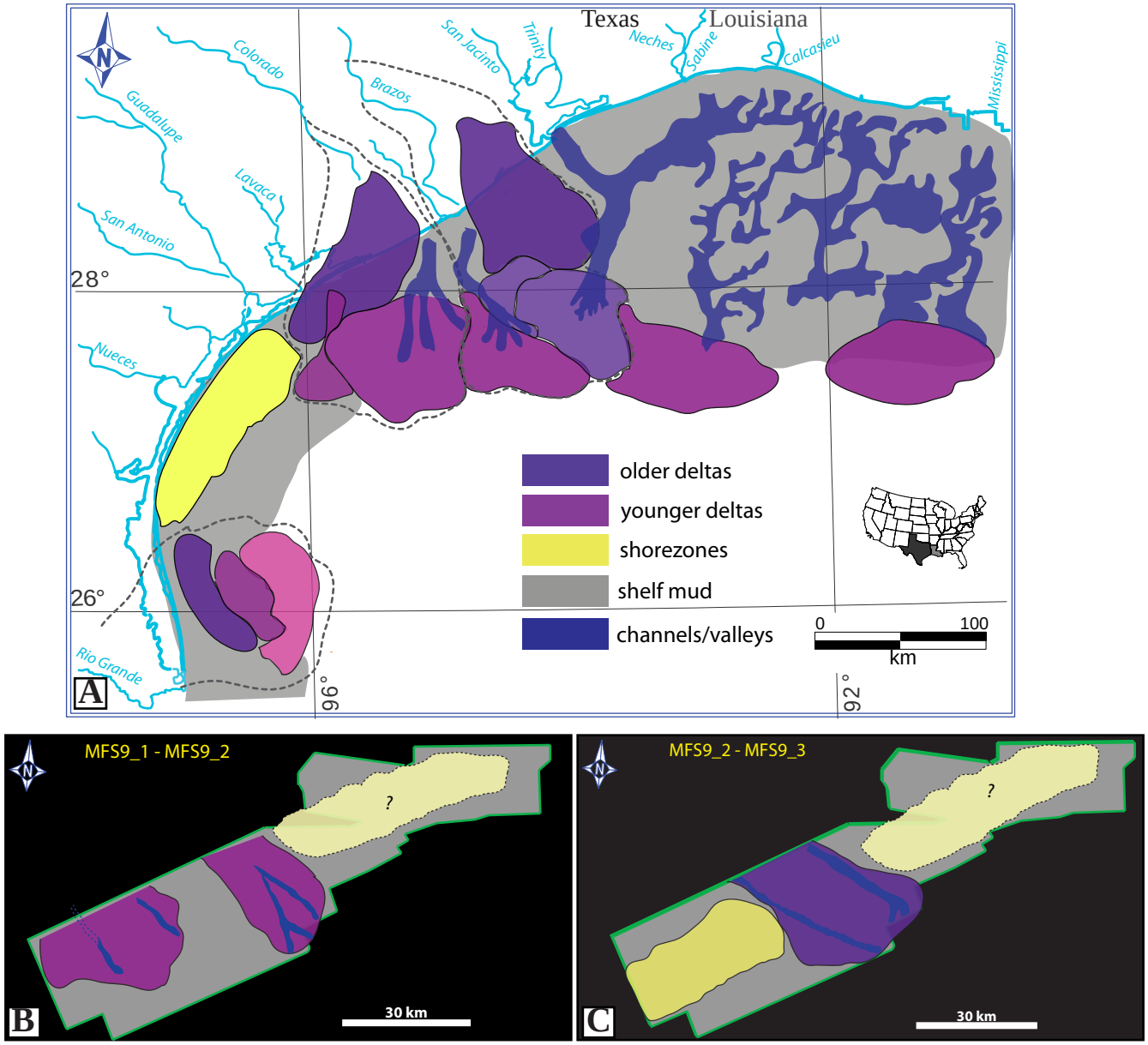

Figure 11. Olariu_et_al.2019